doi:10.20944/preprints202108.0009.v1

Article

Using Cloud-based array electromagnetics on the path to Zero carbon footprint during the energy transition

Kurt Strack[1], Sofia Davydycheva[1], Herminio Passalacqua[2], Maxim Smirnov[1, 3], Xiayu Xu[1]

1 KMS Technologies, Houston, Texas, USA
2 Red Tree Consulting, Houston, Texas, USA
2 Lulea Technical University, Lulea, Sweden

Abstract: One of the key geophysical technologies for the energy industry during energy transition to zero footprint is fluid imaging. Knowledge of fluid distribution allows better, more optimized production reducing thus CO_2 footprint per barrel produced and for CO_2 storage the knowledge of where stored fluids go is mandatory to monitor reservoir seals. Electromagnetic is the preferred way to image fluid due to its strong coupling to the fluid resistivity. Unfortunately, acquiring and interpreting the data takes too long to contribute significantly to field operation and cost optimization. Using artificial intelligence and Cloud based data acquisition we can reduce the operational feedback to near real time and for the interpretation to close to 24 h. This then opens new door for the usefulness of this technology from exploration, monitoring and allows the application envelope to be enlarged to much noisier environment where real time acquisition can be optimized based on the acquired data.

Keywords: CSEM, artificial intelligence, energy transition using electromagnetics, reservoir monitoring, CCUS

1. Introduction

Geophysical fluid imaging technologies are used in a wide range of applications. Since electromagnetics (EM) among geophysical methods determines subsurface resistivities and since resistivity changes are caused primarily by fluid changes, hence, the EM is a prime candidate to address the fluid properties and changes. The biggest potential for EM lies in monitoring geothermal, Carbon Capture and Sequestration, Enhanced Oil Recovery (EOR) of hydrocarbon reservoirs. For EOR of hydrocarbon reservoirs, EM methods increase the recovery factor. At the same time usage of CO_2 flooding to produce the oil, significantly reduce the carbon footprint.

In geothermal applications EM is a standard geophysical method for exploration and monitoring [1]. Monitoring is often carried out in compliance with induced seismicity monitoring and with understanding the fluid movement inside the reservoir. For carbon capture applications only recently EM methods have become of interest [2]. For hydrocarbon applications the EM was in favor in the 1950s, 1960s and1980s, but did not make a breakthrough until marine EM showed its value in the marketplace [3, 4]. With the transition to renewal energy source, we also have to address the carbon reduction by either lower carbon footprint (of existing oil production) or by reinjection of CO_2 in reservoir. Combining these two is called Enhanced Oil Recovery + (EOR +), where we now use CO_2 to drive the enhanced oil production and thus increase the recovery factor.

Thermal EOR is one of the secondary recovery methods that produces the largest environmental impact. In fact, the production of one barrel of Heavy Oil releases to the atmosphere of about 10 kg of carbon dioxide equivalent CO_2e/bbl (assuming the boiling of 3.5 bbls of water for each bbl produced). Optimizing the Steam Oil Ratio (SOR) needed for Thermal EOR by 1% using CSEM (typically improvements are much larger), it is possible to reduce emissions up to 300 thousand kg of CO_{2e}/day (for a global production of 3 MM bbl/day).

Since we now developed EM to be a technology candidate to contribute high value to the future energy transition, we now establish the connection between the measurement methodology and how artificial intelligence would bring significant breakthrough. Simplistically speaking, nothing would be nicer then to have a small sensor that would have a smart phone integrated and we would get the 3D images as answers to our questions. Unfortunately, our signal and methodologies are more complicated. To understand this, we need to understand the issues first:

- A typical signal we measure in the borehole is the magnetic field response to a transmitter at the surface is 400 pT (10^{-12} T). In comparison, the Earth's magnetic field varies between 25,000 to 65,000 nT. A strong refrigerator magnet produces a magnetic field of 10,000,000 nT. As result, adding data transmission or 'noisy' electronics to our very sensitive magnetic sensors is not easy and require many iterations in implementation until high quality measurements are actually available in real time.
- Our geophysical problem, because it is always an inverse problem (going from data to model) is ill-posed, meaning its solution is non-unique. This requires that we understand how data errors, model variations, apriori information and regularization parameters affect multi-parameter sensitivity in 3 dimensions.

Electromagnetic monitoring technology is now well proven [5-8] for hydrocarbon applications while in the 1980s was still in the research phase [6]. The equipment is fully commercial, software algorithms are well tested, and surface measurements confirm in many cases borehole measurements. In order to improve surface-based measurement resolution, borehole sensors can be added. What is needed is demonstration of its value by more applications. For commercial viability, the use of artificial intelligence is essential to optimize operations. Methods were originally developed for land application, but only used in limited cases. The success in the marine EM market proofed the technology value and its commercial viability [8].

We designed a new EM acquisition architecture that combines novel technologies and addresses the need of calibrating surface and borehole data with each other. This is necessary to calibrate surface data to real reservoir scale and parameters. We also add various borehole receivers to the system to improve image focus and resolution [9]. Our array acquisition system applies multiple electromagnetic methods as well as microseismics in ONE layout. This reduces operational cost and provides synergy between the methods. In a production scenario, using multi-component EM allows resolving oil and water-bearing zones equally well as well as getting fluid flow directions. The modular architecture allows a fit-for-purpose configuration tailored to specific exploration/monitoring targets (in terms of depth, frequency range and sensitivity required). The entire system combines hardware with processing and 3D modeling/inversion software, streamlining the workflow for the different methods. 3D feasibility studies leading to acquisition design are routinely carried out – in fact after 35 years those survey where careful feasibility survey design was included in the workflow have always yield exceptional results. This leads to a fully integrated land and borehole acquisition system that can be optimized in a fit-for-purpose fashion and also extended to transition zones and marine acquisition. The core of the system for all units is a unified sensor and system architecture. This alone does not tell us where the biggest technical effort and potential use of artificial intelligence (AI) is. Only when we combine hardware technology with operations, processing and interpretation and go through a realistic project timeline we can see where the potential improvement can be made using AI.

doi:10.20944/preprints202108.0009.v1

Figure 1 shows the workflow for EM reservoir monitoring including technical task and also shows which tasks are the most time consuming. On average the time between repeat surveys is approximately 15 to 18 months. The first step in the workflow is the 3D Feasibility during which we derive survey design and optimized system selection. The main task here is to build a 3D anisotropic model, to benchmark the 3D modeling tools to avoid false anomalies and to run 3D models. The derivation and running of the models and their analysis takes longest (more than 50% of the elapsed time).

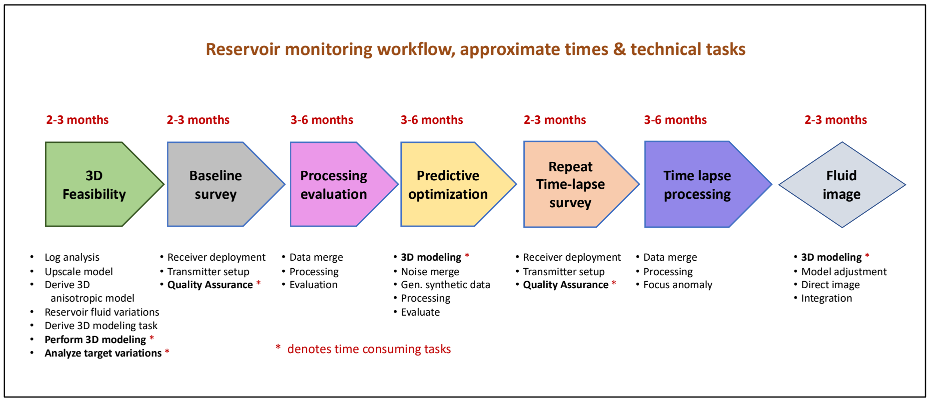

Figure 1. Workflow of a typical electromagnetic reservoir monitoring project. Below the flow block are the major tasks in each step.

During the data acquisition, most of the time is spent on moving of the equipment. Quality Assurance is carried out in parallel to decide if a receiver site is of sufficient quality and recording must continue. For every given day, this process can delay acquisition by the same amount. Quality Assurance includes data processing, basic data interpretation and applying various criteria to examine the data quality. Each of the criteria (like data error and signal length, behavior of the transmitter current) is controllable but in combination they need to be prioritized. The time needed for a baseline survey can often be reduced by using more equipment and automating field operations. The next step includes the data processing and data evaluation, which again mostly depends on careful data administration and data processing that can mostly be further automated. After the data has been evaluated, local noise conditions are known, then the reservoir model and its electromagnetic response is better understood. Having more detailed a priori information makes it meaningful to further optimize for the next repeat survey. We usually add here a step, called predictive optimization, where 3D synthetic data are generated, and local noise is added to the data such that the next repeat survey can be simulated. This allows further survey parameter optimization to ensure better imaging. For the predictive optimization, we have again the 3D modeling time as the biggest elapsed time user. The next step when the time lapse data gets converted to subsurface images includes straight forward processing that can be automated. The last step of producing a verified fluid image again includes time consuming 3D modeling. Throughout the workflow, 3D modeling and Quality Assurance are the most time-consuming tasks and very critical. It would be worthwhile to address them in terms of how they can be made faster and easier using AI.

Before we review where AI is making the biggest impact in electromagnetics for reservoir monitoring, we need to understand where fluid imaging technology makes its contribution to carbon footprint reduction. After that, we describe methodology and instrument and where they fit in the cloud-based acquisition. Then we focus on those parts that benefit most from cloud enabling. Finally, we develop how Cloud based AI can produce

doi:10.20944/preprints202108.0009.v1

game changing technology and contribute to the carbon footprint reduction. This is underscored by some application examples.

2. Value statement: Linking Carbon footprint to fluid imaging

Reducing greenhouse gas emissions has become a primary need for the O&G industry and is reinforced by various national and international agreements. We analyze various parts in the hydrocarbon lifecycle to understand where our technology can make the biggest impact.

On the other hand, the energy needs of the world's population are inescapable. In effect, the International Energy Agency (IEA, 2020) sees that the demand for energy for the year 2040 will increase by 24 % and fossil fuels will supply 74 % of this demand, with a growth of 13 %. The growth of renewable energy sources will reach 83 %.

Hence to continue hydrocarbon production, requires changes (reduction of carbon footprint) to the exploration, production and refining processes to reduce greenhouse gas emissions.

Approximately 90 % of greenhouse gas emissions (CO_2, CH_4, N_2O) are produced in the downstream process. Only 10-20 % of emissions are generated during exploration and extraction. Those emissions reach an average value of 10.3 grams per 1 MJ of crude oil produced [10]. This value may vary depending on the type of hydrocarbon and the process used for its extraction. Table 1 shows the typical emission values according to the types of hydrocarbons and the production stages [11].

OIL TYPE	*UPSTREAM (Kg CO_2e/bbl)*	*MIDSTREAM (Kg CO_2e/bbl)*	*DOWNSTREAM (Kg CO_2e/bbl)*	*Credit/Debit (Kg CO_2e/bbl)*	*Total (Kg CO_2e/bbl)*
Light (Well managed)	35	10	435	-5	475
Heavy Oil (HO)	200	85	450	-20	715
Light (gassy) Oil	375	25	460	-110	750
Extra-Heavy Oil	190	50	515	+15	770

Table 1: Total GHG Emissions for Oil Quality (values from Gordon and Feldmann, 2016) (CO_2e refers to the number of units of CO_2 emissions with the same warming potential as one unit of a different greenhouse gas. CO_2e can be obtained by multiplying the amount of Green House Gas (GHG) by its Global Warming Potential, e.g., one kg of methane is equivalent to 25 kg of CO_2e).

Geophysics can greatly contribute to reducing emissions by supporting cleaner energy production, such as optimizing secondary recovery production that requires flood fluid monitoring (thermal, waterflooding, CO_2).

Likewise, geophysics contributes to the generation and production of clean energies such as Geothermal besides its contribution to its exploration.

An emerging hydrocarbon production technique that will greatly contribute to reducing emissions is the so-called EOR + [12]. EOR + has a dual purpose in that it requires CO_2 capture and sequestration while at the same time part of this CO_2 can be used for enhanced recovery. As such, it is possible not only to reduce emissions by optimizing production, but also to create positive credits by sequestering the excess CO_2 captured

doi:10.20944/preprints202108.0009.v1

from the atmosphere. This enhanced recovery technique requires detailed description of the reservoirs and monitoring of the CO_2 injection front. Both can be achieved with the application of EM methods.

In all these enhanced recovery processes (water, thermal, or CO_2 flooding) the common denominator is the change in electrical resistivity that occurs in the reservoir fluids when water, steam or CO_2 are injected. These resistivity changes, caused by electron flow due to the fluid mobility and conductivity, are detectable with EM methods because in most cases there is a strong resistivity contrast between immobile and mobile fluids.

3. Workflows and value of electromagnetics for fluid imaging

An electromagnetic system is laid out at the surface with transmitter and multiple receivers. Figure 2 shows an example of such a layout where three receiver-lines are used to produce an area coverage. The transmitter in the figure is marked by the yellow lines (4 transmitters in this figure). All receiver locations (shown as circles in the figure) are occupied for each of the transmitters. Usually, before carrying out a survey a feasibility using 3D modeling is done to ensure that the survey setup can see target variations. For that, a resistive log as shown on the right side of the figure is used. It is upscaled to determine a macro anisotropic model. In the figure the upscaled model is shown superimposed on the log on the right: the upscaled horizontal resistivity are in blue and the vertical one in purple. The Earth model on the left shows an even more upscaled anisotropic resistivity model and indicates the target reservoir. In this model the target reservoir could either be the subject to enhanced oil recovery (EOR) or CO_2 injection. Through the transmitter a current of a desired waveform is injected and the response from the induced current in the subsurface is sensed by the receivers. This process is repeated for several hours, and the recorded signals are averaged/stacked to get a better signal-to-noise ratio.

Since the biggest value of electromagnetics is in reservoir monitoring, we use the model of Carlson [13] shown in Figure 3. Here, the fluids are in the pore volume and once stress or strain is experienced on the fluid it causes mobility of the fluid. This mobility makes the electrons in the water saturated part move resulting in drastic resistivity decrease. We often observe that electromagnetic signal goes along with seismic signal from earthquake, and it goes slightly before the seismic signal because the breaking of the grain-to-grain contact comes after the rock experiences stress.

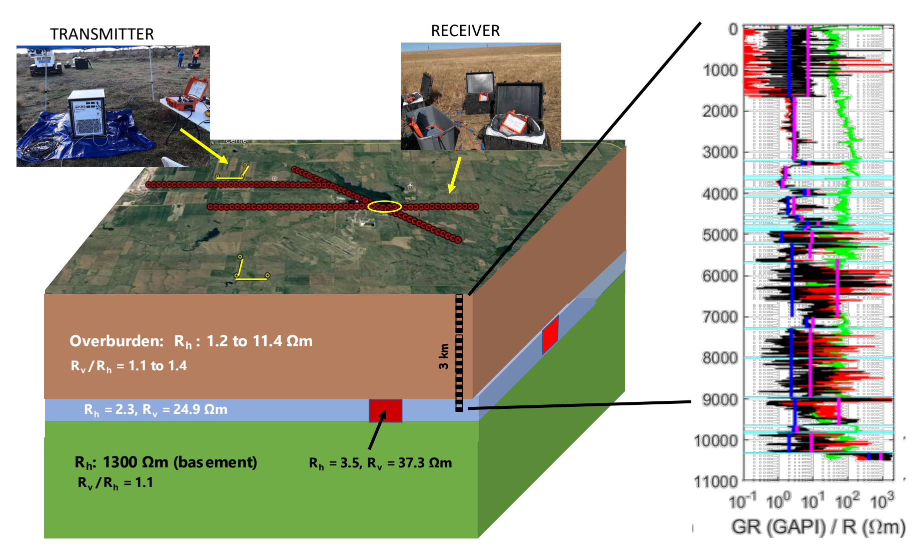

Figure 2. Survey layout for a controlled source EM (CSEM) system showing 4 transmitter locations and three receivers' lines (red). At each location all electromagnetic components are being recorded (after [2]).

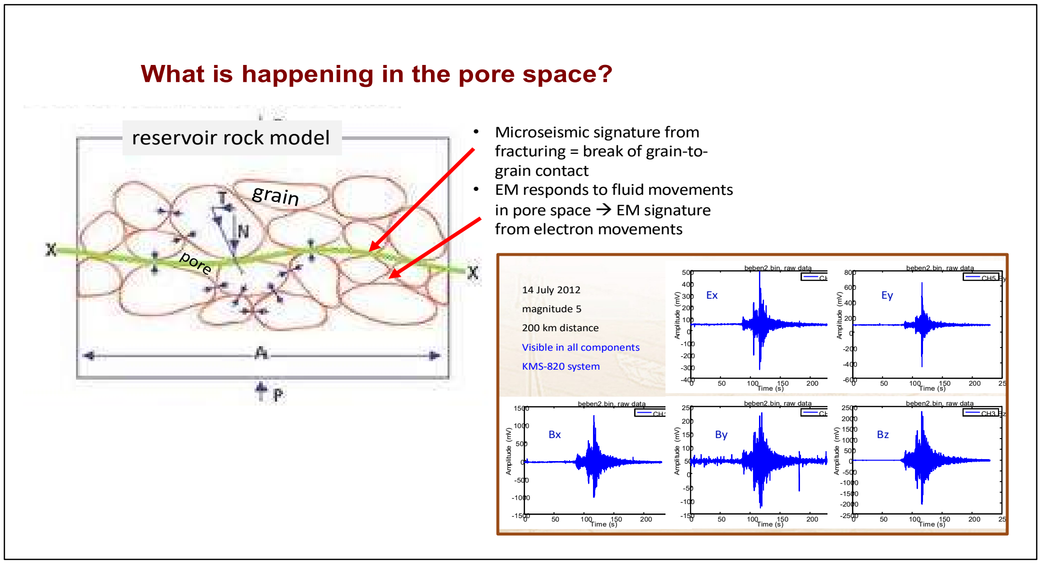

What is happening in the pore space?

- Microseismic signature from fracturing = break of grain-to-grain contact
- EM responds to fluid movements in pore space → EM signature from electron movements

Figure 3. Pore space model based on Carlson [13] showing grains and pore space. The fluids are in the pore space, and the reservoir boundaries are defined by grain-to-grain contact indicated by the green line. When a grain-to-grain contact breaks a seismic signal is sent. Before that the stress and strain on the pore fluid causes mobility and this causes electrons to move dramatically reducing the resistivity of the pore fluid and thus the bulk resistivity. On the right of the figure is an example of an EM signal from an earthquake in India as recording on all 5 components of an EM system. Seeing EM signature (in time) slightly before seismic signature is very typical.

Since we attempt to measure our data better than with the accuracy of 0.5 % (usual calibration variation we observed is between 0.1 to 0.2 %; maximum calibration deviation observed has been around 1.5%) , careful survey design and optimized survey procedures are necessary. A feasibility study is in most cases are mandatory, best even with local noise measurements. For monitoring application, we often look for less than 5% reservoir resistivity variation and we thus recommend a full 3D modeling feasibility study. An example for one is shown in Figure 5. On the left we see the noise spectra for the various sensors (electric and magnetic fields). On the right there are the 3D measured voltages induced in the receiver for various offsets. When we superimpose the noise spectrum as done in Figure 5, we need to stay with our survey design parameters (offset, gains and recording times) above the noise level. For that reason, the superimposed noise was filtered before to simulate realistic situations.

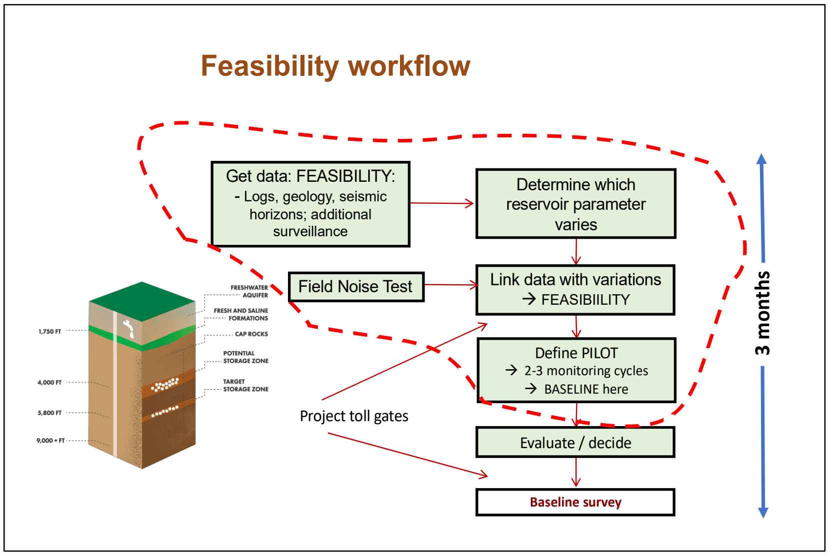

Figure 4. Feasibility workflow of a typical electromagnetic reservoir monitoring project including on-site noise test. The major task is in each block.

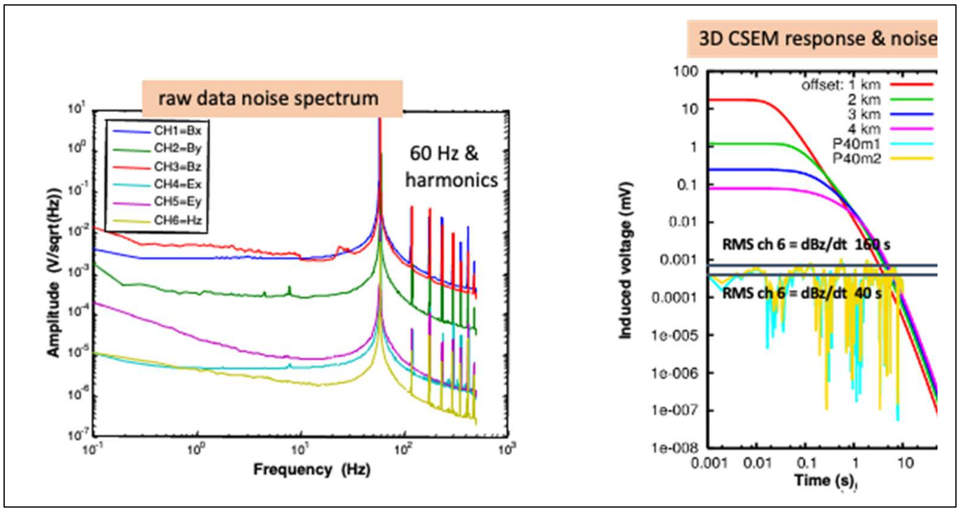

Figure 5. Noise spectra from on-site noise tests for a CSEM monitoring survey (after [2]) on the left. The different curves represent different electromagnetic fields. On the right are measured voltage responses for the magnetic field (dBz/dt) calculated for the 3D model in Figure 1. Superimposed on the right are the noise spectra after filtering. (After [2]). The black horizontal lines are different transmitter current switching periods.

From this we determine recording time and select sensors, survey layout and other operational parameters. Receiver spacings are derived by simulating the receiver response with different spacings. We simulate the time lapse substituting the fluid in the reservoir model and estimating if we can reconstruct the anomalous reservoir.

During the feasibility the most time-consuming part is the 3D modeling and should thus be enhanced by using artificial intelligence as will be discussed below.

Next, we will review the acquisition workflow. Data acquisition is usually an expensive part of a project and requires careful timing and preparation. Figure 6 shows a typical flow diagram for field data acquisition. A potentially time-consuming step is the quality assurance (QA) which is done concurrent to the acquisition. Here, the decision must be made if a receiver is picked up and moved or remain on the ground to get better data (or need to be improved). Thus, getting the data from the receivers to the QA specialist is important. We do this via a noise-free web access box which streams the data to the internet. This allows near real time QA decision.

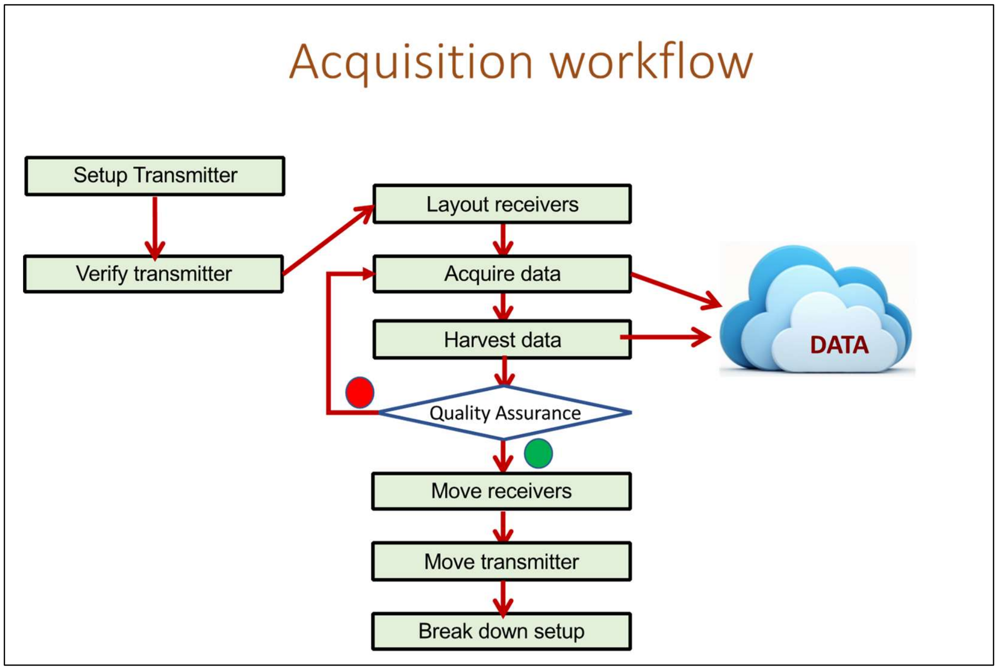

Figure 6. Acquisition workflow of a typical CSEM reservoir monitoring project. Quality assurance decisions are marked with red (NO GO) and green (GO) dots. The data is sent directly from the instrument to the Cloud.

4. Background enabling instrumentation

The electromagnetic signals that we measure to obtain information of the subsurface are very small (tens to several hundred pT) and they need to be measured in the presence of an Earth's magnetic field (25,000 to 65,000 nT) that is 1 million time bigger. In addition, we have external noise and man-mad noise that can be more than 1000 times larger than the Earth magnetic field. Simply said: a difficult task but not impossible and customary to geophysics/military/space science. The sensors have such high sensitivity that they cannot be easily integrated with other data transmitting devices such as cell phone as they generate too much noise in the sensor and distort the signal. For passive electromagnetic this is more difficult because of the broadband nature of the signal than for controlled source electromagnetics but still the issue remains. So, often data transmission is done during acquisition pauses. For CSEM that is not easily possible because we require a very accurate

doi:10.20944/preprints202108.0009.v1

reference voltage level which can only be obtained with continuous data acquisition. Figure 7 shows the typical noise density for various magnetic field sensors (the electric field sensors have different issues) used for land geophysical methods discussed here. In comparison we also plotted the noise density for an earthquake prediction coil and the noise density of the natural magnetic fields. Obviously, all sensors must be below that noise level. We solve this issue by jumping via a low noise wifi connection a short distance away from sensors and all analog parts into a web access box where the data is buffered and then sent to the internet with various protocol. Further discussion is in the section below.

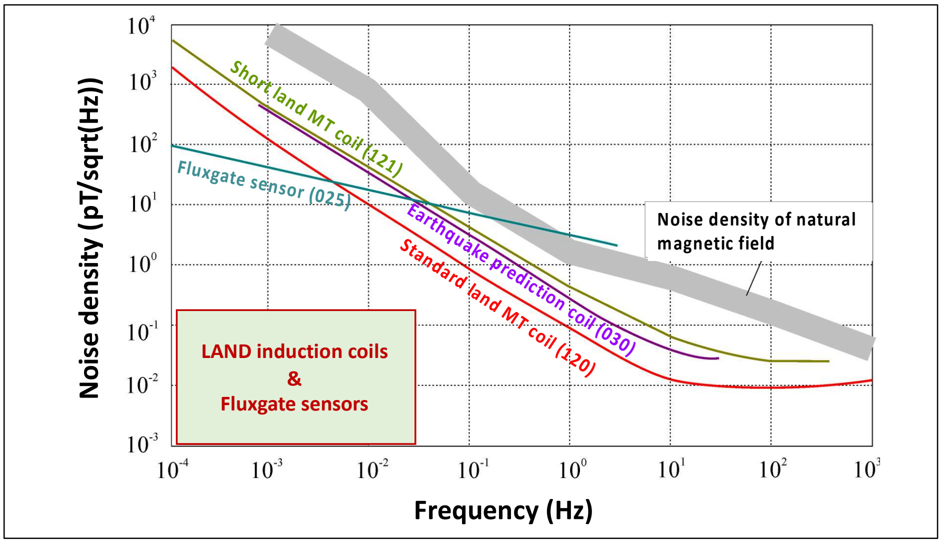

Figure 7. Noise density of various land sensors (fluxgate and induction coils) compared with an earthquake prediction sensor and the Earth's magnetic field noise density

Figure 8 shows field images of various receiver equipment components. Target depth is between 500 m to 6 km in almost any geologic environment. At each of the sites multicomponent EM equipment is deployed to measure either magnetotelluric (MT) or Controlled Source ElectroMagnetics (CSEM) response. We use ultra-stable electrodes for the electric field that have a broadband response from close to DC (better than <0.0001 Hz) to about 40 kHz on the high end. Stability of the sensors at the low frequency end is essential for fidelity of the signal and to determine the proper reference voltage. It should be noted that capacitive electrode is not suitable as they do not go low enough in frequency. At the top left of Figure 8 we show the electrode we used which is a lead-free LEMI-701. The electrode spacing is either 50 or 100 m. Magnetic field measurements can be done by either fluxgate sensors, induction coils (center photo in Figure 8) or air loop (bottom left photo). We test all of them at each survey location and compare its noise with the local noise to optimize layout and acquisition times including operational deployment. Pictures of the acquisition system we use (KMS-820 array system) are shown in the other three photographs in the figure. The yellow box in the picture on the top right is the web access box that allows data streaming to the Cloud. It is important to note that the acquisition system must operate from -20^0 C to 60^0 C, acquire continuous data for weeks at a time and be connectable to the Cloud.

Figure 9 shows various transmitter photographs under field conditions. The transmitter consists of a generator, a current switchbox and a waveform controller that record the transmitter signals and is GPS synchronized. On the top left of the figure and the center bottom are pictures of our 150 KVA (KMS-5100 - 150) switchbox, back and front side, respectively. The switchbox converts the AC current from the generator to DC and switches it according to a predefined waveform (usually a square wave). This current (up to 400 A) is injected into the ground via large grounding electrode plates placed in to pits on both sides of an approximately 1 km long thick cable. A picture of four pits (one dipole side) is shown in the top center of Figure 9. Further transmitter site picture is on the top right (generator and observer trailer on the top right) and on the bottom left a camp site in an oil field. In Figure 9, center right, is a picture of the 100 KVA version of the switch box and below on the right an inside view of the recording trailer.

The most important element in all of this is to send the data in real time to the Cloud. Where cellular phone coverage is available this can be done via cell phone.

Figure 8. Pictures of the various electromagnetic sensors and acquisition systems in field settings. At the top left is an electrode used for the electric field measurements. At the top center is the acquisition system near a power plant followed on the top right followed by a closer view of the system, web access box and battery in a field container. Below on the bottom right are several systems during attest with seismic 3-component geophones connected. In the center is a magnetic field sensor (induction coil) and on the bottom left a magnetic field sensor implemented by a large multi-turn air loop.

doi:10.20944/preprints202108.0009.v1

Figure 9. Field images of various component of the transmitter equipment. At the top left is the power connection of the 150 kVA transmitter switch box (back view). Its front view in the field is shown in bottom center. At the top venter are pictures of the electrode puts where the current injecting electrode are buried. At the top right is a view of the 150 kVA generator and observer trailer (switch box is inside) used for 24 hours continuous for 5 weeks operation partially at minus 20^0 C. An inside view of the trailer is at the bottom right. On the left side is a transmitter site set up as camp in the tropic in an oil field.

Having described the instrument [14], we need to consider briefly the methods they can be used for. The most mature electromagnetic method is magnetotelluric (MT) as described in [15-18]. MT is the primary methods for geothermal but also used to limited extend for hydrocarbon and other academic applications. MT uses the Earth's natural field, and the signal can be improved by adding a signal to the weak band. In that mode the method is known as Controlled Source AudioMagnetoTellurics or CSAMT [19]. An even better coupling to the resistivity of the subsurface is obtained when the equipment is used in Controlled Source EM or CSEM mode (time or frequency domain) [20-22]. The problem with CSEM is that the image focus is unknown. This can be improved by using focusing methods like the borehole-logging-style focusing described by Rylinskaya and Davydycheva [23]. Using such a system for a combination of methods including boreholes is described by He et al. [24] and Strack [25] and for marine by Constable [26]. The choice of methodology is determined by finding the optimum solution using the 3D Feasibility approach described above.

5. Converting the workflow to Cloud-based application

On the path to a fully distributed autonomous system where sensors, acquisition, and Cloud data transfer is fully integrated we still need to honor small electromagnetic signals and their sensitivity to external noise – natural or man-made. To separate between data for storage/transmittal purposes, service support and deep learning related analytics we separate the Cloud into three layers: the DATA layer which is mostly for data transmission and archival purposes, the OPERATIONS layer where interaction between acquisition unit and user occurs and the IMAGE layer where the information is interpreted and improved using deep learning algorithms. In the OPERATIONS layer feedback between acquisition unit and the user also occurs. When the web access box is placed away from the sensor both respective curves are very similar (left of bottom of Figure 10). Clearly, the web-access box generates little to no extra noise and let us realize the value of having the field data available in real time. It should be mentioned that for magnetotelluric data it is important to separate the acquisition unit from the web access box by a few meters.

The most difficult part in this is the cell phone coverage and good data transfer. While replacing of the Sim card should be the standard, we experience a lot of inconsistency between cell phone providers around the globe and must work often with their technician to make this work. Hopefully once satellite-based internet is commonly available this will become history.

Operationally, having the data available in near real time in the Cloud, is a huge time and thus money saving. Collaboration between staff on site and the experts located sometimes half a globe away is much more immediate and beneficial not only during problem solving instances. An obvious advantage is that the data can be processed quickly while the equipment is still laid out on the ground.

While it is obviously an enabling operational benefit to have the instruments deliver the data in real time, in the Reservoir Monitoring (which we determined is the highest value for electromagnetics in the future path to Zero footprint), we need to look at most time critical task indicated in Figure 1. During the 3D Feasibility step, 3D modeling is the most time consuming, while the analysis of the results only requires more experience to automate the process in the operation Cloud layer.

Usually, when we think about 3D modeling and data we think about inversion because we are trying to derive an Earth model from the data. Because our field measurement contains noise, and our methods are partially multi-valued we cannot always provide a unique inverse solution. When analyzing this problem with borehole resistivity logs in the 1990 [27, 28], we noticed that 95 % of the computing resource are spent on the 3D forward model, which has a unique solution. So, instead of using the neural net for the inversion it was more effective for the forward models [29], where it also can save up to 95 % of the computing time. Subsequent substitution neural net based forward modeling reduce the inversion elapse CPU time by 92 %. When replacing forward models with neural nets, we must realize that EM responses depend on resistivity contrast and the conductance or transverse resistance of the specific reservoir unit. This is often called equivalence in electromagnetics. This has fundamental implications as resistivity profiles are usually specific for each specific basin (or formation analogue). Not only will artificial intelligence-based algorithm need to be trained for each basin (or geologic analogue) but also with many training sets (tens of thousands). Figure 11 describes the inversion components for electromagnetics. In the forward modeling the Earth model (1D or 3D) gets combined by the forward modeling function and model responses are generated. These are then compared with the real data and if they match, we have found a realistic model explaining the data. Since they usually do not match in the initial iterations, the forward modeling is done may times and thus becomes the 95 % CPU time eater. It can easily be substituted by artificial neural networks. The input to inversion is the data from the Cloud data layer and the output would go to the image layer. Figure 12 explains why we do not recommend substituting the inversion (better model match/updating) with a neural net. In the figure we have two parameter spaces that represent the model or transformed parameter space [20]. For a 30-layer model we have 29-layer parameter (one-dimensional) or 29^3 parameters in the three-dimensional case plus various vector anisotropies. Because the response of electromagnetics is to conductance (thickness time conductivity product) or transverse resistance (resistivity time thickness product), we often cannot separate parameter combinations and obtain error surface as in Figure 12 that have local and global minima. From geophysical viewpoint, we always look for the global minimum, which may not always be the right thing to do from the explorationist viewpoint where we are trying to get a consistent model with most data sites and accept higher curve fitting errors. That decision between local and global minimum is not easy as it requires understanding of all data sets and geology.

doi:10.20944/preprints202108.0009.v1

==

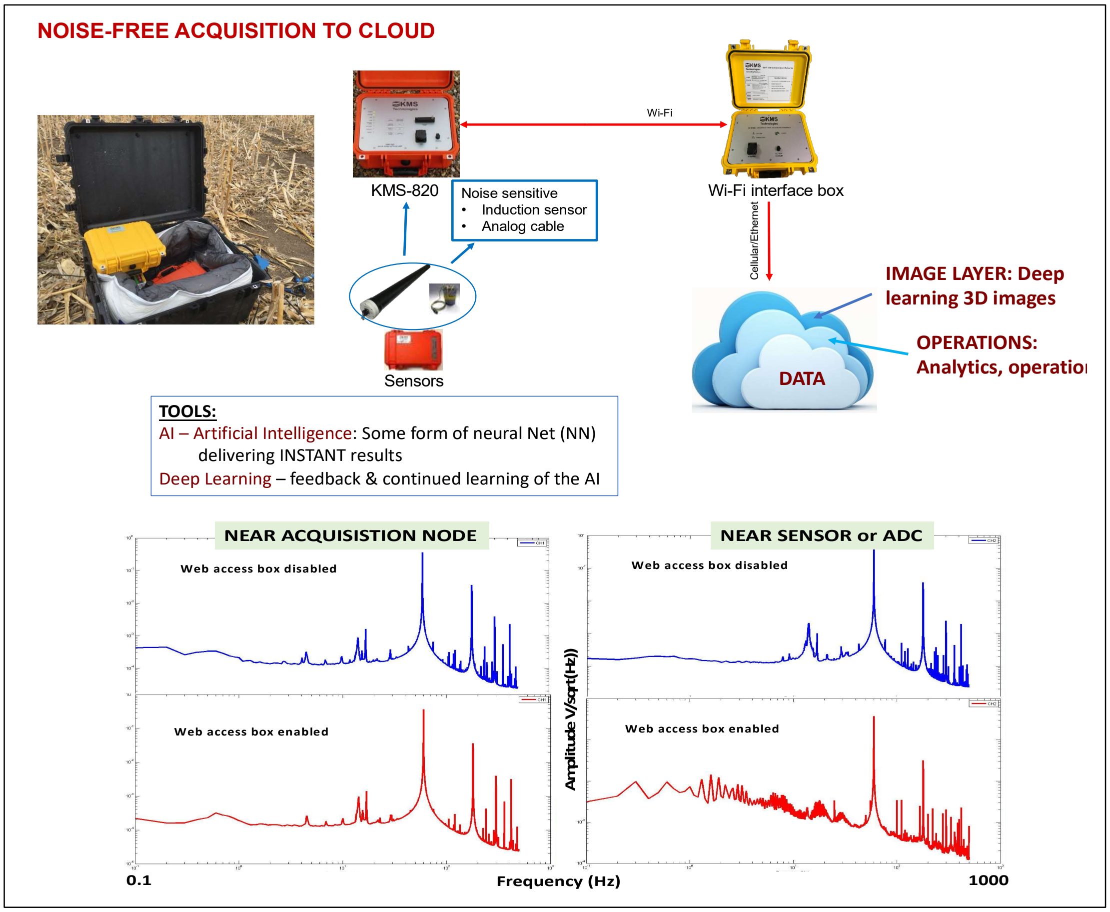

TOOLS:
AI – Artificial Intelligence: Some form of neural Net (NN) delivering INSTANT results
Deep Learning – feedback & continued learning of the AI

Figure 10. Process flow of electromagnetic data directly to the Cloud (top half) and a data example illustration the noise improvement using a noise-free web access box (bottom half). On the top left is the acquisition system with the web access box (yellow box) that is placed away (20 m) from the sensitive magnetic field sensor displayed in the pictorial flow diagram below the acquisition unit. From the web access box (WI-FI interface in the figure) the data is sent to the Cloud via cell phone, and wireless connection or wired LAN. The plots below show the frequency spectra of data recording with and without web access box and close to the magnetic field sensor (right side) versus away from the sensor.

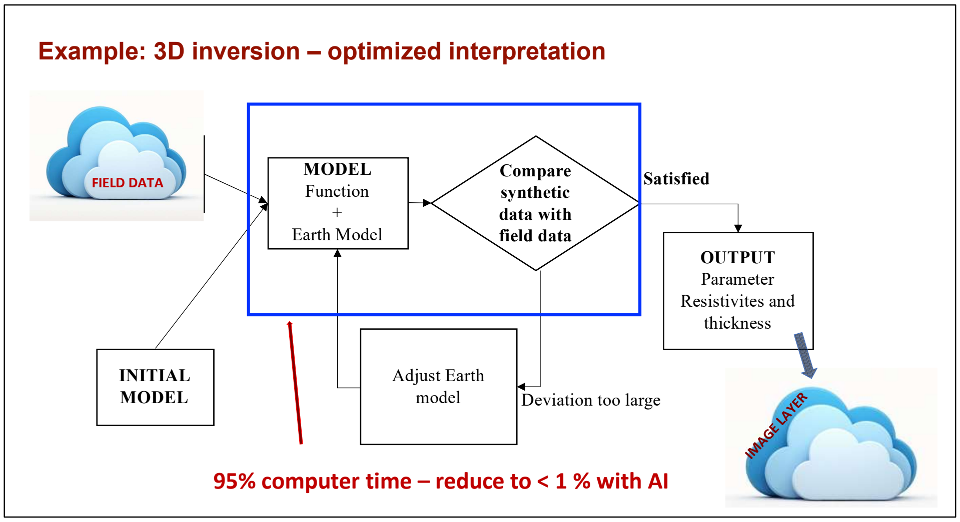

Figure 11. Inversion flow diagram dissecting the forward modeling from the model adjustments and Cloud interaction. The input come from the DATA layer and the out goes to the IMAGE layer of the Cloud.

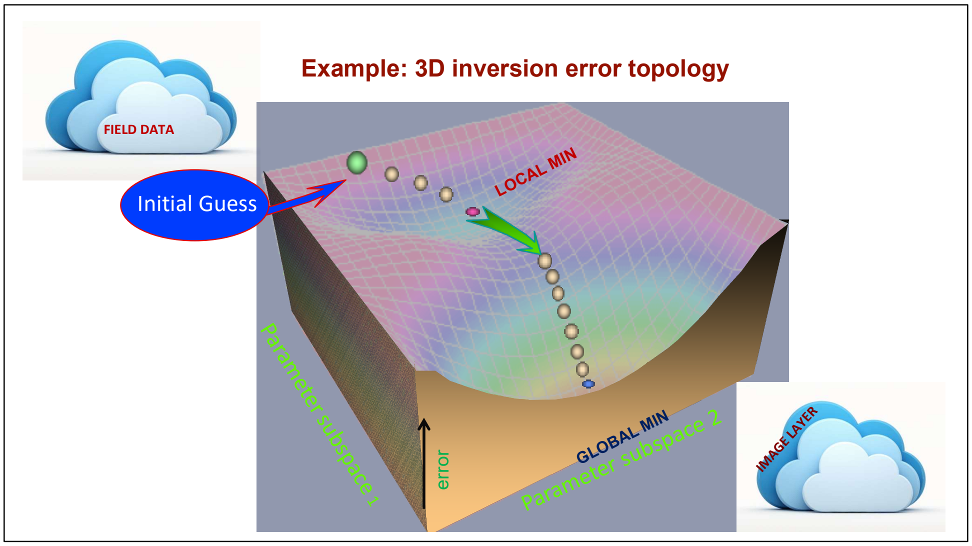

Figure 12. Multi-parameter error surface illustrating how the initial guess model moves around the error surface towards a global solution. If we follow strict convergence criteria it could get stuck around the local minimum. The axis parameter represents only two parameters of the model.

6. Implementation example

To illustrate the application of converging to artificial intelligence application, we applied the above-mentioned principles to the instrumentation and deliver the data directly to the Cloud. In Figure 1, we describe the most time-consuming parts and here we select some of them to illustrate the value of the implementation.

Obviously, the Cloud usage as data delivery and depository vehicle saves a lot of time /money. Figure 13 shows an example of electromagnetic data (here MT data) where the Cloud enable us to combine data sets acquired thousands of miles apart. We acquired a large set of MT data in the Northern USA and used two remote reference sites [16], one in the Northern USA 600 km away from the survey area and another in the Southern USA about 3000 km away. Using the Cloud allows us to utilize interpretation resources far away. In this case the data acquisition was done in the USA at -200 C at two locations and around 50 C at the Southern US location. The interpretation was done in Europe (Sweden and Germany) and Texas. The results were available within 24 hours. This would not have been possible without the noise-free web access as described above. Figure 12 shows the results and comparison between using a single site and including a remote reference site. In the individual site processing, we still see a significant mismatch over a wide frequency band. When including the remote reference site this mismatch goes away as we get more realistic data. To the right of the curves are the Earth models obtained from the inversion (dashed) and the one derived using upscaling of the resistivity log shown in Figure 2. The inversion results match the log well. The value in this is multi-fold:

- Significant interpretation time saving.
- For operations purposes, we determine easier which site needs to be repeated and which one does not.
- Significantly confidence increase in the 3D Feasibility subsurface model reducing interpretation time

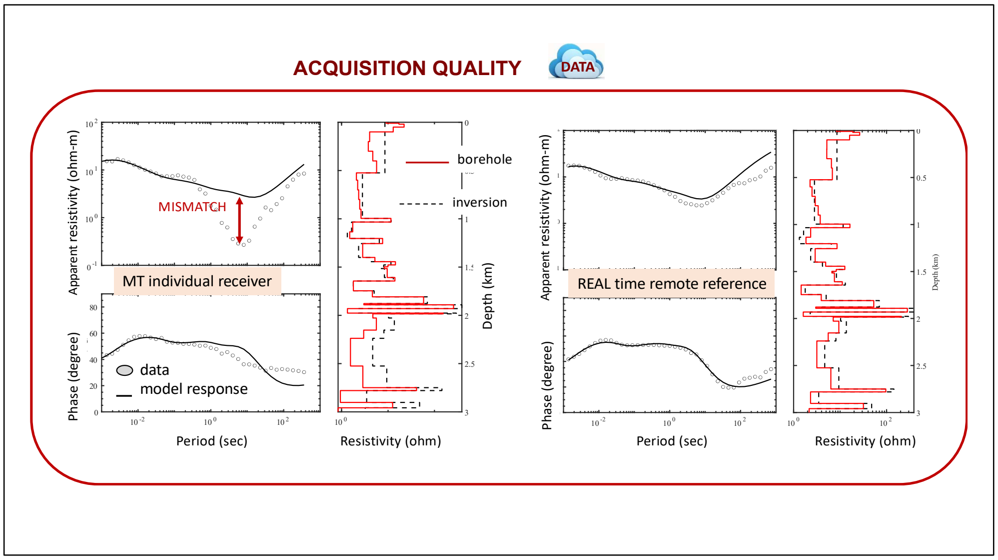

Figure 13. Comparison of magnetotelluric (MT) data using an individual site for processing and including data from a remote reference site. The top rows show apparent resistivities and the bottom phase responses. Synthetic curves are the solid lines, and the dots are the field data. On the right the Earth models derived from the 3D anisotropic are displayed in comparison with the borehole upscaled log.

As next step, we developed a deep learning neural network to assist our data Quality Assurance (QA) effort, mostly because the turn-around time of the quality assessment can be very costly for operations. It is part of NOISE-FREE acquisition to cloud, which is explained in Figure 10. To automate and improve QA process, we introduce deep learning network and implement the process in three steps: STEP 1. Set up a dedicated server to harvest each data set from the cloud; STEP 2. Run deep learning neural network to derive instance QA result; STEP 3. Feedback to operator and add to the operations Cloud layer. The success of this implementation relies on build a suitable neural network and get it trained by deep learning method [31, 32, 33]. For illustration purposes we illustrate here the initial AI learning phase.

Data QA comes from acquisition observation, raw data curve behaviors and 1D inversion results. Since we had an accurate anisotropic model the inversion fits overriding acquisition quality. Thus, we define two levels of QA parameters: Level 1 is based on acquisition observation and raw data curve behaviors; Level 2 is based on 1D inversion results. To simplify, we use QA 1 to refer to QA parameter Level 1, and QA 2 refers to QA parameter Level 2. In QA 1, MT curves are evaluated together within the frequency range from 0.001 to 1000 Hz. QA 1 is a robust processing parameter [44]: Root mean square (RMS) error, Phase behavior, and apparent resistivity. QA 1 was set to classify each curve into 4 levels:

- Level 1- Excellent, ≥ 85 % of data points have a relative error (STD of Amplitude/Amplitude; absolute error of phase = 0.56 relative error for amplitude) < 10 % and with smooth continuity.
- Level 2 - Good - more than 75 % of data point (in period) have a relative error < 20 %
- Level 3 - Acceptable – Phase does not go out of a quadrant (0 – 90°) (minimum) and amplitude of impedance tensor does not go down more than 45^{0}and it is not increasing with period
- Level 4 - Poor, data points show large dispersants, and it is impossible to define a curve for interpretation.

Further categorization is possible based on the impedance tensor (main components) and will be implemented in future deep learning practice.

In QA 2, 1D Inversion quality criteria – override (if inversion quality is better than acquisition quality including remote reference is taken precedence)

- Level 1 - Excellent, data fitting has a Normalized Root Mean Square fit (RMSf) ≤ 2.
- Level 2 - Good, 1D fitting has a Normalized Root Mean Square fit (RMSf) > 2 and ≤ 5.
- Level 3 - Acceptable, 1D data fitting has a Normalized Root Mean Square fit (RMSf) > 5 and ≤ 10.
- Level 4 - Poor, 1D data fitting has a Normalized Root Mean Square fit (RMSf) > 10

We use Normalized RMS fit which is RMS (fit between predicted observed)/STD to fit the data within 1: i.e., fits the data within standard error bars [18].

Deep learning algorithm is able to learn patterns from data sets. During a magnetotelluric project in US, we acquired about 240 data sets in 48 stations. We are using these 240 data sets into two steps: training step and testing step. Deep learning program train itself through training data and test accuracy of the algorithm via testing data and that would be done later as the value impact is smaller in the operational value context.

We randomly selected 37 data sets as training data and rest of data sets are testing data. For each training data set, we randomly defined a predicted QA result to simulate of the output of neural network, and predicted result is compared with actual QA result. This comparison ends up with an error (different between predicted QA result and actual QA result) and difference ratio (error divides actual QA result). Then error and difference ratio are used as input value to a statistical quality control model [34] of training neural network. This statistical quality control model is based on theory of central limit theorem [35], it removes outlier of predicted QA when training neural network and improves neural network.

Figure 14 shows the backpropagation (BP) network in this application [36]. In this BP network, three input nodes are GPS information (including coordinates, time, and altitude), gain setting (acquisition unit amplifier setting for each channel), and operator’s name from each data sets; two hidden layers are QA 1 (QA parameter Level 1) and QA 2 (QA parameter Level 2); One output node is predicted QA result. The predicted QA result will get compared with actual QA result, which produced by experienced geophysicist. The comparison is quality controlled by central limit theorem algorithm [35], which explained below. By feeding comparison result back to BP network, BP network is getting trained continuously and the deep learning cycle starts. The more data sets we provide to this BP network, the better it performs.

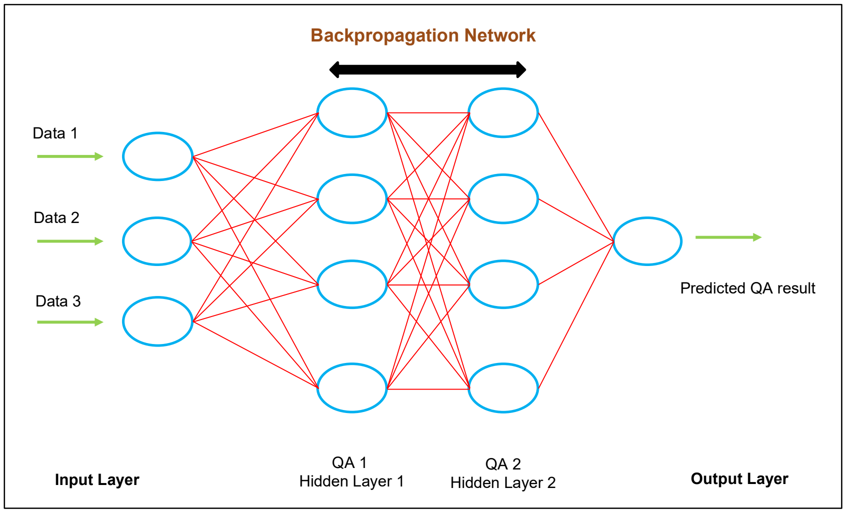

Figure 14. BP network to train and predict QA results. There are three input nodes, which are GPS information (including coordinates, time, and altitude), gain setting (acquisition unit amplifier setting for each channel), and operator's name This BP network has two hidden layers. First layer (QA 1) is robust processing parameters: Root mean square (RMS) error, Phase behavior, and apparent resistivity. Second layer (QA 2) is 1D inversion result Root mean square fit (RMSf) error. Output node is predicted QA result, and it will get compared with actual QA result.

To improve our BP network, we need to establish a statistical quality control model [34] to fine-tune deep learning predicted results. Deep learning network predicted results, especially at the beginning stage, will have large error rate. We set up an outlier detection algorithm based on central limit theorem [35]. The quality control model is explained in Figure 15.

The difference for the data set means the difference between predicted QA result and actual QA result (Equation 1), and difference ratio is difference divides actual QA result (Equation 2).

$$Difference = Predicted\ QA\ result - Actual\ QA\ result \quad (1)$$

$$Difference\ Ratio = \frac{Difference}{Actual\ QA\ result} \quad (2)$$

According to central limit theorem, the following four properties are needed and calculated from sample training data sets:

1. Mean of sample ($\mu_{\bar{x}}$) mean equals to the mean of whole data sets

$$\mu_{\bar{x}} = \mu \quad (3)$$

2. The standard deviation of the sample ($\sigma_{\bar{x}}$) equals to deviation of whole data set divided by square root of the sample size

$$\sigma_{\bar{x}} = \frac{\sigma}{\sqrt{n}} \quad (4)$$

3. We assume the original data sets are normally distributed, therefore, the sample means will be normally distributed

4. If, in any case, the distribution of original data sets is not normal, a sample size of 30 or more is needed to use a normal distribution to approximate the distribution of the sample means. The larger the sample, the better the approximation will be.

We selected 37 sample data sets shown in Figure 15 (left) as initial input to quality control model for BP network. The 37 data sets are selected from 37 stations (one data set from each station). Due to operational issues or high cultural noise at certain locations, only 37 stations out of 48 planned sites are recorded and interpreted. Each of these selected sample data set has a random predicted QA result. According to central limit theorem [35], we calculate mean of the sample means $\mu_{\bar{x}} = 19.59$, and standard deviation of sample mean $\sigma_{\bar{x}} = 24.61$. We defined upper control limit (UCL) and as well as lower control limits (LCL). The limit is range within $\mu \pm 3\sigma$, which is from -54.24 to 93.42. When we are feeding our training data sets to BP network, if difference ratio of one data set is out of the range (-54.24 to 93.42), we consider this data set is an outlier and it will be removed. According to our test it covers 99 % of predicted results but it can still remove outliers. By implementing this central limit theorem as a quality control model, all the data points outside of limit range will be consider outlier and removed. As we feed more training data sets to BP network and quality control predicted results, our deep learning neural network will get better to produce instant predicted QA results.

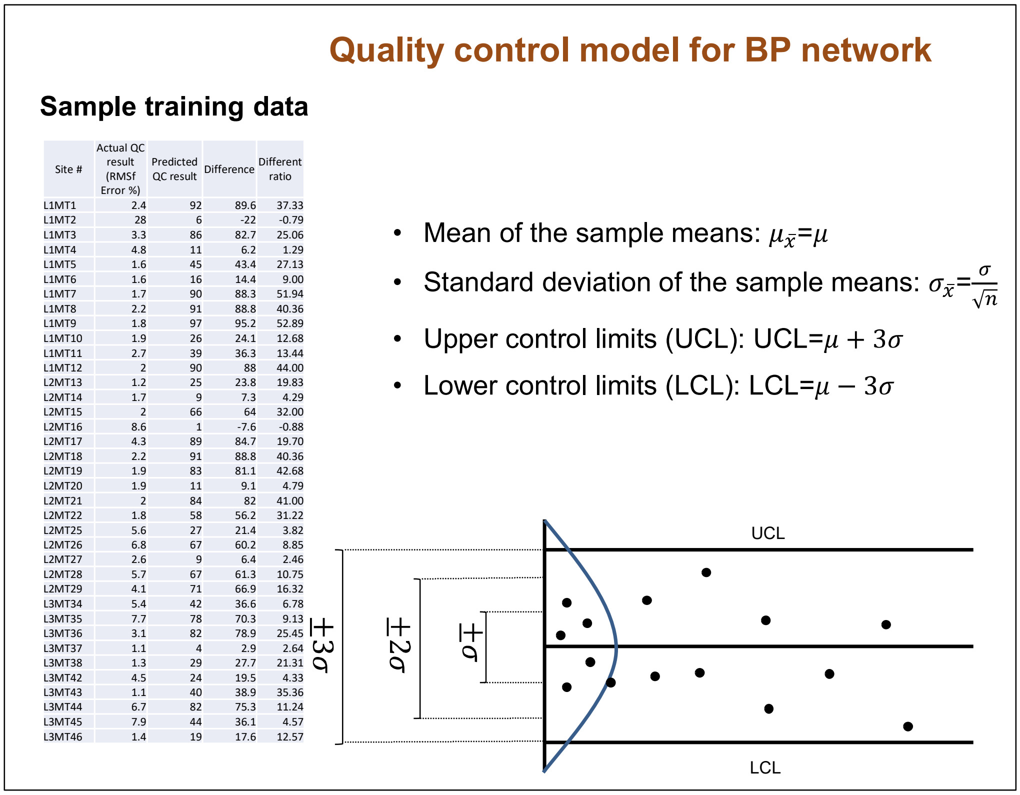

Quality control model for BP network

Sample training data

Site #	Actual QC result (RMSf Error %)	Predicted QC result	Difference	Different ratio
L1MT1	2.4	92	89.6	37.33
L1MT2	28	6	-22	-0.79
L1MT3	3.3	86	82.7	25.06
L1MT4	4.8	11	6.2	1.29
L1MT5	1.6	45	43.4	27.13
L1MT6	1.6	16	14.4	9.00
L1MT7	1.7	90	88.3	51.94
L1MT8	2.2	91	88.8	40.36
L1MT9	1.8	97	95.2	52.89
L1MT10	1.9	26	24.1	12.68
L1MT11	2.7	39	36.3	13.44
L1MT12	2	90	88	44.00
L2MT13	1.2	25	23.8	19.83
L2MT14	1.7	9	7.3	4.29
L2MT15	2	66	64	32.00
L2MT16	8.6	1	-7.6	-0.88
L2MT17	4.3	89	84.7	19.70
L2MT18	2.2	91	88.8	40.36
L2MT19	1.9	83	81.1	42.68
L2MT20	1.9	11	9.1	4.79
L2MT21	2	84	82	41.00
L2MT22	1.8	58	56.2	31.22
L2MT25	5.6	27	21.4	3.82
L2MT26	6.8	67	60.2	8.85
L2MT27	2.6	9	6.4	2.46
L2MT28	5.7	67	61.3	10.75
L2MT29	4.1	71	66.9	16.32
L3MT34	5.4	42	36.6	6.78
L3MT35	7.7	78	70.3	9.13
L3MT36	3.1	82	78.9	25.45
L3MT37	1.1	4	2.9	2.64
L3MT38	1.3	29	27.7	21.31
L3MT42	4.5	24	19.5	4.33
L3MT43	1.1	40	38.9	35.36
L3MT44	6.7	82	75.3	11.24
L3MT45	7.9	44	36.1	4.57
L3MT46	1.4	19	17.6	12.57

- Mean of the sample means: $\mu_{\bar{x}}=\mu$
- Standard deviation of the sample means: $\sigma_{\bar{x}}=\frac{\sigma}{\sqrt{n}}$
- Upper control limits (UCL): UCL=$\mu + 3\sigma$
- Lower control limits (LCL): LCL=$\mu - 3\sigma$

Figure 15. Quality control model for BP network. Create central limit algorithm base on selected sample training data. This model is used to remove outlier of predicted QA result and feed back to BP network for improvement of training purpose. The table on the left side is 37 selected training data sets. Text and formula in the middle are calculated values of statistical quality control model. Diagram on the bottom explains how this quality control model removes outlier.

Once the quality control model for our BP network is setup, we started feeding data to train the BP network. We randomly selected data sets of 37 stations (one data set from each station, exactly same amount of data sets as our initial sample data sets). BP network training process takes time, especially at the beginning stage. By feeding training data sets into the BP network in multiple iterations, we expect to get better predicted QA results gradually. As shown in Figure 16, training result of first iteration (table on the left in Figure 16) shows average difference is 45.09 and average different ration is 19.96. After 10 iterations, training result turns out to be average difference is 11.20 and average different ratio is 5.28. From this comparison, we can see there are about 75 % improved predicted QA results after iterations of training. It is very promising that as we are feeding more training data sets to our BP network, better predicted QA results will be produced.

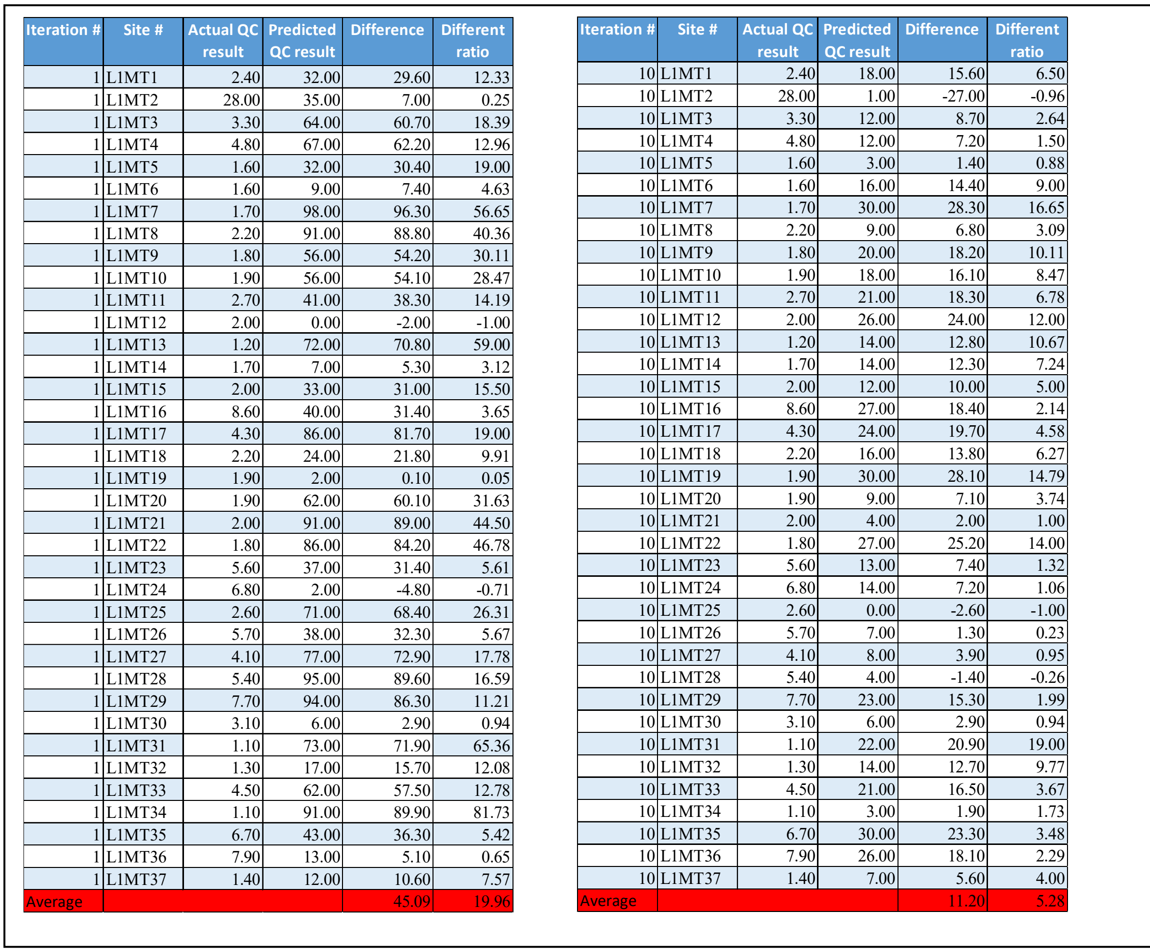

Iteration #	Site #	Actual QC result	Predicted QC result	Difference	Different ratio
1	L1MT1	2.40	32.00	29.60	12.33
1	L1MT2	28.00	35.00	7.00	0.25
1	L1MT3	3.30	64.00	60.70	18.39
1	L1MT4	4.80	67.00	62.20	12.96
1	L1MT5	1.60	32.00	30.40	19.00
1	L1MT6	1.60	9.00	7.40	4.63
1	L1MT7	1.70	98.00	96.30	56.65
1	L1MT8	2.20	91.00	88.80	40.36
1	L1MT9	1.80	56.00	54.20	30.11
1	L1MT10	1.90	56.00	54.10	28.47
1	L1MT11	2.70	41.00	38.30	14.19
1	L1MT12	2.00	0.00	-2.00	-1.00
1	L1MT13	1.20	72.00	70.80	59.00
1	L1MT14	1.70	7.00	5.30	3.12
1	L1MT15	2.00	33.00	31.00	15.50
1	L1MT16	8.60	40.00	31.40	3.65
1	L1MT17	4.30	86.00	81.70	19.00
1	L1MT18	2.20	24.00	21.80	9.91
1	L1MT19	1.90	2.00	0.10	0.05
1	L1MT20	1.90	62.00	60.10	31.63
1	L1MT21	2.00	91.00	89.00	44.50
1	L1MT22	1.80	86.00	84.20	46.78
1	L1MT23	5.60	37.00	31.40	5.61
1	L1MT24	6.80	2.00	-4.80	-0.71
1	L1MT25	2.60	71.00	68.40	26.31
1	L1MT26	5.70	38.00	32.30	5.67
1	L1MT27	4.10	77.00	72.90	17.78
1	L1MT28	5.40	95.00	89.60	16.59
1	L1MT29	7.70	94.00	86.30	11.21
1	L1MT30	3.10	6.00	2.90	0.94
1	L1MT31	1.10	73.00	71.90	65.36
1	L1MT32	1.30	17.00	15.70	12.08
1	L1MT33	4.50	62.00	57.50	12.78
1	L1MT34	1.10	91.00	89.90	81.73
1	L1MT35	6.70	43.00	36.30	5.42
1	L1MT36	7.90	13.00	5.10	0.65
1	L1MT37	1.40	12.00	10.60	7.57
Average				45.09	19.96

Iteration #	Site #	Actual QC result	Predicted QC result	Difference	Different ratio
10	L1MT1	2.40	18.00	15.60	6.50
10	L1MT2	28.00	1.00	-27.00	-0.96
10	L1MT3	3.30	12.00	8.70	2.64
10	L1MT4	4.80	12.00	7.20	1.50
10	L1MT5	1.60	3.00	1.40	0.88
10	L1MT6	1.60	16.00	14.40	9.00
10	L1MT7	1.70	30.00	28.30	16.65
10	L1MT8	2.20	9.00	6.80	3.09
10	L1MT9	1.80	20.00	18.20	10.11
10	L1MT10	1.90	18.00	16.10	8.47
10	L1MT11	2.70	21.00	18.30	6.78
10	L1MT12	2.00	26.00	24.00	12.00
10	L1MT13	1.20	14.00	12.80	10.67
10	L1MT14	1.70	14.00	12.30	7.24
10	L1MT15	2.00	12.00	10.00	5.00
10	L1MT16	8.60	27.00	18.40	2.14
10	L1MT17	4.30	24.00	19.70	4.58
10	L1MT18	2.20	16.00	13.80	6.27
10	L1MT19	1.90	30.00	28.10	14.79
10	L1MT20	1.90	9.00	7.10	3.74
10	L1MT21	2.00	4.00	2.00	1.00
10	L1MT22	1.80	27.00	25.20	14.00
10	L1MT23	5.60	13.00	7.40	1.32
10	L1MT24	6.80	14.00	7.20	1.06
10	L1MT25	2.60	0.00	-2.60	-1.00
10	L1MT26	5.70	7.00	1.30	0.23
10	L1MT27	4.10	8.00	3.90	0.95
10	L1MT28	5.40	4.00	-1.40	-0.26
10	L1MT29	7.70	23.00	15.30	1.99
10	L1MT30	3.10	6.00	2.90	0.94
10	L1MT31	1.10	22.00	20.90	19.00
10	L1MT32	1.30	14.00	12.70	9.77
10	L1MT33	4.50	21.00	16.50	3.67
10	L1MT34	1.10	3.00	1.90	1.73
10	L1MT35	6.70	30.00	23.30	3.48
10	L1MT36	7.90	26.00	18.10	2.29
10	L1MT37	1.40	7.00	5.60	4.00
Average				11.20	5.28

Figure 16. BP network training results comparison. Left table is training result of first iteration, on the bottom, average difference is 45.09 and average Different ratio is 19.96. Right table is training result after 10 iterations, on the average difference is 11.20 and average difference ration is 5.28. Thus, we can see while our BP network getting trained, better predicted result it produces.

Our work combined deep learning networks and statistical quality control model to make fast turnaround predication of MT QA results. As far this method has already shown us that it has great potential to reduce field geophysicist workload and significantly improve efficiency of field operation in terms of data quality feedback. As part of our cloud acquisition workflow, we continue to train our BP network to produce faster and better predicted QA results. Meanwhile, we are also adding fully automated feature to have this QA results delivered to field crew's fingertip simultaneously. This will significantly improve field operation decision making process, make field logistic more efficient, and thus reduce operational cost effectively.

Thus far we discuss using AI in data delivery and quality assurance, both very time consuming and costly. We also outlined the roadmap for effective implementation in 3D modeling, as illustration example we look at the value the Cloud enabled, AI supported technology provides by looking at its enabling capability in predictive optimization and performing repeat time-lapse surveys. During the energy transition a high value target for GHG reduction are heavy oil (HO) applications to EOR. We have taken a typical HO example which includes a shallow reservoir which is of near-term concern but also environmentally sensitive due to its shallow depth. Without the above-described technology and workflows this application would be extremely difficult to accomplish. With it we can apply new technologies that we explain forthcoming.

The production of HO can produce up to 715 kg CO_2e/bbl from upstream to downstream, of which 10 kg CO_2e/bbl are released when thermal methods are applied. Monitoring of steam injected becomes extremely critical to lower the number of emissions. Resistivity can change up to 150 % for a temperature increase of 100^{O} C.

Several feasibility studies were carried out in the last decade [37, 38] and we present below selective results one of these in this context.

Figure 17 shows the geologic section of a representative heavy oil field. Depending on the resistivity contrast between the fluids in the reservoir we will use different EM sensors. Simultaneous Microseismic data is also acquired to monitor the changes of pressure occurring in the reservoir due to the injection of steam on one side. On the other side this will be used to observe potential breaks of the reservoir seals. In the figure we show the resistivity model of the formations and the saturation fluid description. Also shown is the CSEM survey configuration. We did not show the anisotropic model to avoid distraction from the purpose here on improving image focus and delivering the data in near real time.

We carried out a simulation of the EM responses using a 3D finite-difference method [39] applying to the feasibility concepts described above and in [20, 40]. In Figure 18 we show the synthetic response of the offset-corrected horizontal electric field (Ex), for the isotropic (left) and the anisotropic case (right). We assumed here a vertical resistivity Rv= 8 ohm-m and a horizontal resistivity Rh = 4 ohm-m. Cleary, as expected, the anisotropy adds significantly to the anomaly. Henceforth, we will only use the anisotropic model. We also can see from this figure that the anomalous behavior or difference between flooded and unflooded reservoir is largest near the reservoir (outline at the bottom of the graphs). This suggest if we can get this difference out of the data using some type of transformation that only show the variation between adjacent receivers, we might just see this [40]. This is commonly done in focused borehole measurements and can be translated to surface electrical fields [41, 42].

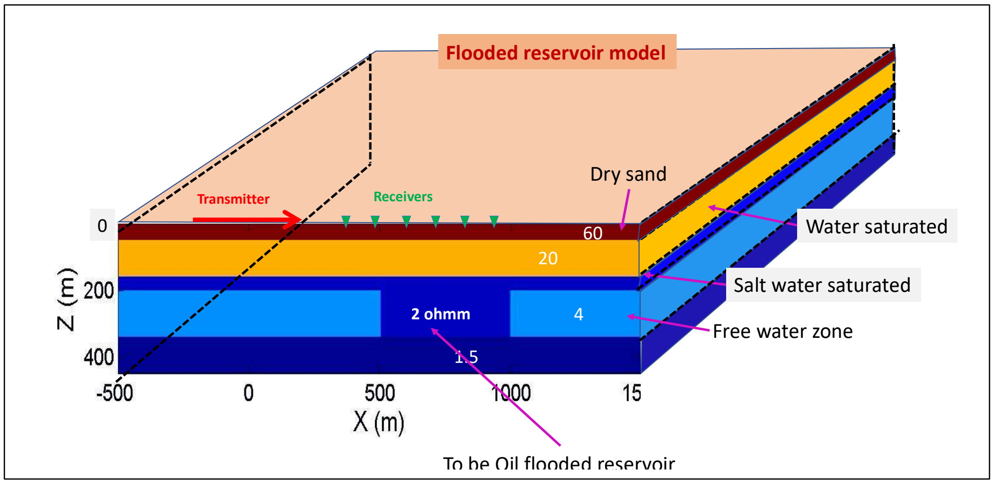

Figure 17. Simplified geologic model of a heavy oil (HO) reservoir. The HO section is the reservoir shown here as salt water saturated .

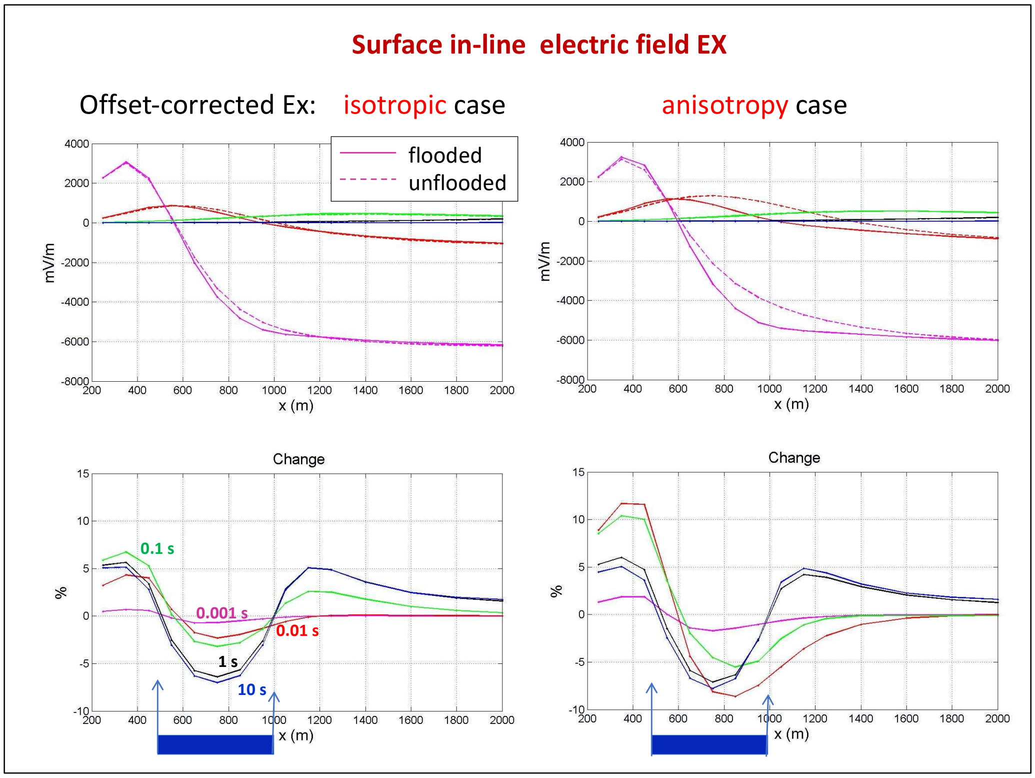

Figure 18. Horizontal Electric field response as a function of the distance from the transmitter (left) using the isotropic model on from Figure15. On the right, we added anisotropy to the model resistivities [modified after 40].

Figure 19 show two other electromagnetic field components to achieve this anomaly enhancement, one is the measurement of the vertical field and one the measurement of the horizontal magnetic field time-derivative. The implementation of the vertical electric field measurement would happen via a shallow vertical borehole tool, that get buried in

doi:10.20944/preprints202108.0009.v1

20 m deep boreholes. This leads directly to the befits of using artificial intelligence and Cloud services.

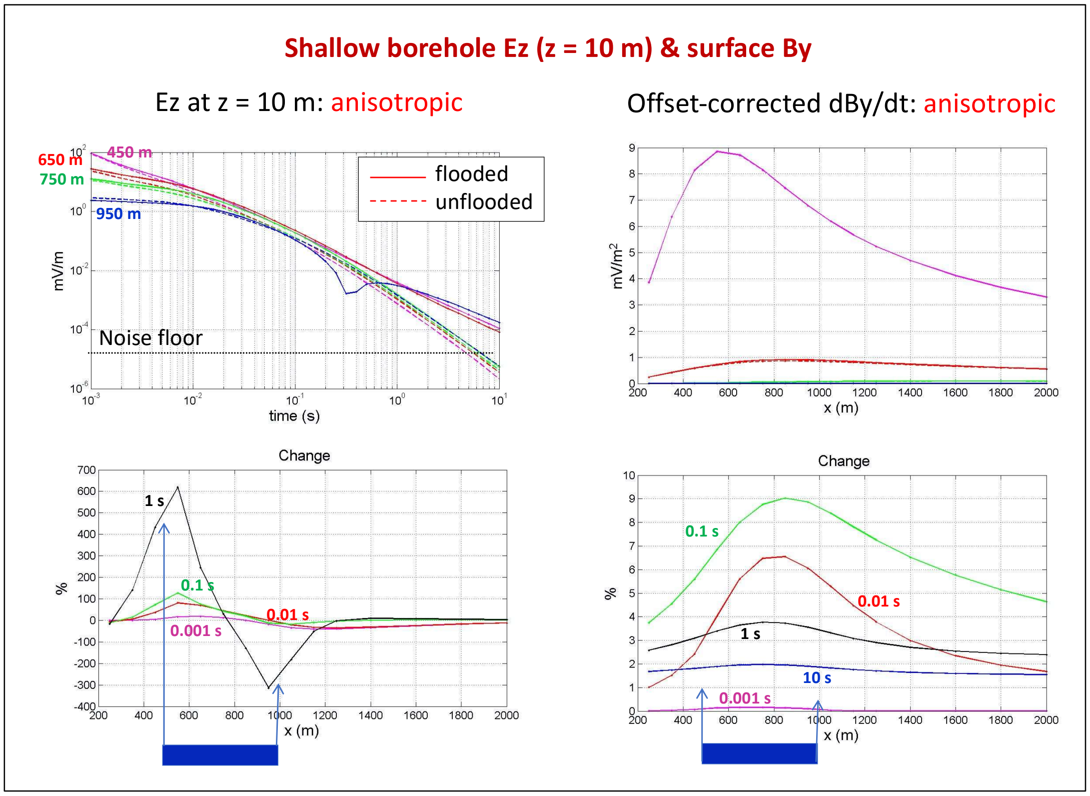

Figure 19. Comparison of two types for measurement that lead to focusing methodology. On the left are the vertical electric field measured in a shallow borehole (leads to shallow borehole tool described in text). On the right are the anomalous responses at various offsets for the horizontal magnetic field time-derivative (leading to differential measurements).

The electromagnetic components and method discussed are more sensitive to thin horizontal resistors/reservoir with hydrocarbon saturation. The key value proposition is reducing operations cost (firstly injected steam cost, secondarily EOR-recovery factor improvement of 20-30 %). So, this means we need the data very soon after acquisition to improve the steam injection operations plan. The highest value lies in data turn-around time going to nearly real time. If we assume large number of receiver installation in a HO steam flood operation, necessity to get result at the latest 24 h later, the steps are:

- Immediate data transmission to the CLOUD of receiver and noise-compensating reference receivers
- Real time QA to be fed to time-section interpretation (primary: display transformation can be done in near-real time with operator control).
- Client receives decision make steam maps to produce optimization operation variations.

Clearly, after some time the operator interaction can be aided by deep learning.

7. Conclusion

Using artificial intelligence in the workflow can greatly help to bring complex decisions closer to the data acquisition operations. The biggest value is in faster operations and making decision at a time when they can impact acquisition data quality.

We selected electromagnetic geophysical equipment with the application of fluid monitoring which is important for the energy transition. In particular in the EOR+ scenario we can address lower carbon footprint of heavy oil production and CO_2 injection at the same driving this energy resource faster to Zero footprint.

Since electromagnetic depends on very low signal it is also sensitive to noise and sending the data noise-free to the Cloud is non-trivial but essential to make near real time operating decisions.

Since we do not know the explicit structure and resistivities of the reservoir, we need to acquire all electromagnetic components as each has a bias to certain parts of the geoelectric section. Only directional multi-component measurements give you a clear description of the anisotropic model.

While the operational value of including AI in the electromagnetic workflow is greatest, further value assessment shows that HO applications and fluid monitoring could hardly be done without it.

Author's contributions: K. Strack: lead author, concepts and technology details; S. Davydycheva: 3D modeling; H. Passalacqua: EOR and GHG research; M. Smirnov: cloud-based quality assurance algorithm, guidance and architecture; X. Xu: cloud-based AI software implementation.

Acknowledgements: We acknowledge the support and contribution of T. Hanstein, and Y. Martinez throughout the development. KMS Technologies gave us permission to publish this material.

References

1. Gasperikova, E., and Cumming, W., How geophysics can help the geothermal industry. Society Exploration Geophysicists, Technical Program Expanded Abstracts, 2020, 3379-3383, https://doi.org/10.1190/segam2020-3425875.1.
2. Barajas-Olalde, C., Davydycheva, S., Hanstein, T., Laudal, D., Martinez, Y., MacLennan, K., Mikula, S., Adams, D.C., Klapperich, R.J., Peck, W.D., and Strack, K., Using controlled-source electromagnetic (CSEM) for CO2 storage monitoring in the North Dakota CarbonSAFE project. Society Exploration Geophysicists, Technical Program Expanded Abstracts, 2021,
3. Strack, K.M., Future Directions of Electromagnetic Methods for Hydrocarbon Applications. Surveys in Geophysics, 2014, 35, 157-177, DOI: 10.1007/s10712-013-9237-z.
4. Streich, R., Controlled-Source Electromagnetic Approaches for Hydrocarbon Exploration and Monitoring on Land. Survey in Geophysics, 2016, 37, 47-80, DOI: 10.1007/s10712-015-9336-0.
5. Henke, C. H., Krieger, M., Strack, K., and Zerilli, A., Subsalt imaging in Northern Germany using multi-physics. Interpretation, 2020, 8, SQ14-SQ24, DOI: 10.1190/INT-2020-0026.1.
6. Strack, K.-M., Lebrocq, K., Moss, D. C., Petry, H., Vozoff, K., and Wolfgram, P. A., Case histories of long-offset transient electromagnetics (LOTEM) in hydrocarbon exploration. First Break, 1989, 7, 467-477, DOI: 10.3997/1365-2397.1989027.
7. Strack, K., and Pandey, P.B., Exploration with controlled-source electromagnetic under basalt cover in India. The Leading Edge, 2007, 26, 268-27, DOI: 10.1190/1.2715056.
8. Berre, L., Morten, J.P., Baillie, G., and Nerland, E., Experience on controlled-source electromagnetic performance for exploration in Norway. Interpretation, 2020, 8, SQ25-SQ37, DOI: 10.1190/INT-2019-0307.1.
9. Strack, K., Davydycheva, S., Hanstein, T. and Smirnov, M., A New Array System for Multiphysics (MT, LOTEM, and Microseismic) with Focus on Reservoir Monitoring, GeoEM 2017 conference Bandung Indonesia - invited keynote, AIP Conference Proceedings 1861, 020001 2017, DOI: 10.1063/1.4990887
10. Masnadi, M.S., El-Houjeiri, H.M., Schunack, D., Li, Y., Englander, J.G., Badahdah, D., Monfort, J.C., Anderson, J.E., Wallington, T.J., Bergerson, J.A., Gordon, D., Koomey, J., Przesmitzki, S., Azevedo, I.L., Bi, X.T., Duffy, J.E., Heath, G.A., Keoleian, G.A., McGlade, C., Meehan, D.N., Yeh, S., You, F., Wang, M., and Brandt, A.R., Global carbon intensity of crude oil production. Science, 2018, 361, 851, DOI: 10.1126/science.aar6859
11. Gordon, D., and Feldman, J., Breaking Down the Barrel: Tracing GHG Emissions Through the Oil Supply Chain, Carnegie Endowment for International Peace, Washington DC, 2016, https://carnegieendowment.org/2016/02/09/breaking-down-barrel-tracing-ghg-emissions-through-oil-supply-chain-pub-62722.

12. International Energy Agency (IEA), Storing CO2 through Enhanced Oil Recovery. International Energy Agency Carbon Capture Unit, Paris, 2015, https://www.iea.org/reports/storing-co2-through-enhanced-oil-recovery.
13. Carlson, M.R., An Analysis of the Caprock Failure at Joslyn, SPE Heavy Oil Conference in Calgary, Alberta, 12-14th June 2012, SPE-156962-PP, DOI: 10.2118/156962-MS
14. Jiang, J., Aziz, A.A., Liu, Y. and Strack, K.M., 2015, Geophysical Acquisition System, US Patent 9,057,801.
15. Vozoff, K., The magnetotelluric method in the exploration of sedimentary basins, Geophysics, 1972, 37, 98-141.
16. Vozoff, K., The magnetotelluric method, in Nabighian, M. N., Ed., Electromagnetic methods in applied geophysics, Society of Exploration Geophysics, 1991, 2B, 641-711, DOI: 10.1190/1.1444178.
17. Simpson, F., and Bahr, K., Practical Magnetotellurics, 2005, Cambridge University Press, DOI: 10.1017/CBO9780511614095.
18. Chave, A.D., and Jones, A.G., The Magnetotelluric Method, Cambridge University Press, 2012, 10.1017/CBO9781139020138
19. Zonge, K. L., and Hughes, L. J., Controlled source audio-frequency magnetotellurics, in Nabighian, M. N., Ed., Electromagnetic methods in applied geophysics, Vol. II, Society Exploration Geophysicists, 1991.
20. Strack, K.M., Exploration with deep transient electromagnetics. Elsevier, 1992, 373 (reprinted 1999).
21. Keller, G. V., Pritchard J.I., Jacobson, J.J., and Harthill, J.N., Megasource Time-Domain Electromagnetic Sounding Methods, Geophysics, 1984, 49, 993-1009, DOI: 10.1190/1.1441743.
22. Kaufman, A. A. and Keller, G.V., Frequency and transient soundings, Elsevier Science Publishers B.V., 1983, DOI: 10.1111/j.1365-246X.1984.tb02230.x.
23. Rykhlinskaya, E., and Davydycheva, S., Method for marine geoelectrical exploration with electrical current focusing, 2014, U.S. Patent 8,762,062 B2.
24. He, Z., Liu, X., Weiting, W. and Zhou, H., Mapping reservoir boundary by borehole-surface TFEM: Two case studies. The Leading Edge, 2006, 24, 896-900, DOI: 10.1190/1.1839725
25. Strack, K.-M., Integrated borehole system for reservoir detection and monitoring, 2003, US Patent US 06670813 .
26. Constable, S., Review paper: Instrumentation for marine magnetotelluric and controlled source electromagnetic sounding, Geophys. Prosp., 2013, 61, 505-532, DOI: 10.1111/j.1365-2478.2012. 01117.x
27. Vallas, H.A., Mezzatesta A., and Strack, K.-M., Resistivity-Log Inversion Using a Heterogeneous Artificial Neural Network, SEG 63rd Annual Meeting and International Exhibition, 1993, Paper WS7.2 , 1395, DOI: 10.1190/1.1822416
28. Zhang, L., Poulton, M.M., and Wang, T., Borehole electrical resistivity modeling using neural networks, Geophysics, 2002, 67: 1790-1797, DOI: 10.1190/1.1527079
29. Strack, K.M., Fast 3D inversion of electromagnetic survey data using a trained neural network in the forward modeling branch, 2009, US 7574410 .
30. Passalacqua, H. and Strack K., Reducing Carbon Footprint by Geophysical Monitoring of EOR Processes, SEG International Exhibition and 90th Annual Meeting, 2020, DOI: 10.1190/segam2020-3424907.1
31. Bengio, Y., Courville, A., and Vincent, P., Representation Learning: A Review and New Perspectives, IEEE Transactions on Software Engineering, 2013, 35 (8): 1798–1828, DOI: 10.1109/TPAMI.2013.50
32. Schmidhuber, J., Deep Learning in Neural Networks: An Overview, Neural Networks, 2015, 61: 85–117, DOI: 10.1016/j.neunet.2014.09.003
33. Bengio, Y., LeCun, Y., and Hinton, G., Deep Learning, Nature, 2015, 521 (7553): 436–444, DOI: 10.1038/nature14539
34. Dai, W., Yoshigoe K., and Parsley, W., Improving Data Quality Through Deep Learning and Statistical Models, In Information Technology-New Generations, 2018, 515-522, DOI: 10.1007/978-3-319-54978-1_66
35. Bárány, I., and Vu, V., Central limit theorems for Gaussian polytopes, Annals of Probability. Institute of Mathematical Statistics, 2007, 35 (4): 1593–1621, DOI: 10.1214/009117906000000791
36. Goodfellow, I., Bengio, Y., and Courville, A., 6.5 Back-Propagation and Other Differentiation Algorithms, MIT Press, 2015, 200–220.
37. Passalacqua, H., Boonyasaknanoon, P., and Strack, K., Integrated Geophysical Monitoring for Heavy Oil, SPE-184089, Heavy Oil Conference, 2016, Kuwait, Kuwait: DOI: 10.2118/184089-MS
38. Passalacqua, H., Davydycheva, S. and Strack, K. Feasibility of multi-physics reservoir monitoring for Heavy Oil, 2018, Heavy Oil Conference Kuwait, SPE-193690-MS, DOI: 10.2118/193690-MS
39. Davydycheva, S., and Druskin, V., Staggered grid for Maxwell's equations in arbitrary 3-D inhomogeneous anisotropic media, in: Oristaglio, M., and Spies, B., Eds. Three-dimensional electromagnetics: Society Exploration Geophysicists, 1999, 119-137.
40. Strack, K., and Davydycheva, S., Using electromagnetics to map lateral fluid variations in carbonates in SE Asia, in Purenovic, J. (ed), New Approaches in Engineerung Research, 2, 2021, Book Publisher International., 2021, DOI: 10.9734/bpi/naer/v2/8202D
41. Davydycheva, S., Method and apparatus for detecting and mapping subsurface anomalies, 2018, U.S. Patent 9891339 B2.
42. Davydycheva, S., and Rykhlinski, N, Focused Source electromagnetic survey versus standard CSEM: 3D modeling in complex geometries, Geophysics, 2011, 76, F27-F41.
43. Donat, A., Untersuchungen der magnetischen Horizontalkomponenten bei long-offset transient electromagnetics (LOTEM), Diplom thesis, Inst. f. Geophysik u. Meteorologie, 1996, University of Cologne.
44. Smirnov, M., Magnetotelluric data processing with a robust statistical procedure having a high breakdown point, Geophysical Journal International, 2003, 152, 1, DOI: 10.1046